Journal of Materials Chemistry A

Ce stabilized Ni-SrO as a catalytic phase transition sorbent for integrated CO2 capture and CH4 reforming

Journal:	*Journal of Materials Chemistry A*
Manuscript ID	TA-ART-11-2021-009967.R1
Article Type:	Paper
Date Submitted by the Author:	20-Dec-2021
Complete List of Authors:	Gu, Haiming; Southeast University, School of energy and enviroment Gao, Yunfei; North Carolina State University, Chemical Engineering Iftikhar, Sherafghan; North Carolina State University, North Carolina State University, Chemical and Biomolecular Engineering Li, Fanxing; North Carolina State University, Chemical Engineering

ARTICLE

Ce stabilized Ni-SrO as a catalytic phase transition sorbent for integrated CO_2 capture and CH_4 reforming

Received 00th January 20xx,
Accepted 00th January 20xx

DOI: 10.1039/x0xx00000x

Haiming Gu [a,b] , Yunfei Gao [a,c,*], Sherafghan Iftikhar [a] and Fanxing Li [a, *]

Integration of carbon dioxide capture from flue gas with dry reforming of CH_4 represents an attractive approach for CO_2 utilization. The selection of a suitable bifunctional material serving as a catalyst/sorbent is the key. This paper reports Ni decorated and CeO_x-stabilized SrO ($SrCe_{0.5}Ni_{0.5}$) as a multi-functional, phase transition catalytic sorbent material. The effect of CeO_x on the morphology, structure, decarbonation reactivity, and cyclic stability of the catalytic sorbent was determined with TEM-EDX, XRD, *in-situ* XRD, CH_4-TPR and TGA. Cyclic process tests were conducted in a packed bed reactor. The results indicate that large Ni clusters were present on the surface of the SrNi sorbent, and the addition of CeO_2 promoted even distribution of the Ni on the surface. Moreover, the Ce-Sr interaction promoted a complex carbonation/decarbonation phase-transition, i.e. $SrCO_3 + CeO_2 \leftrightarrow Sr_2CeO_4 + CO_2$ as opposed to the conventional, simple carbonation/decarbonation cycles (e.g. $SrCO_3 \leftrightarrow SrO + CO_2$). This double replacement crystalline phase transition mechanism not only adjusted the carbonation/calcination thermodynamics to facilitate $SrCO_3$ decomposition at relatively low temperatures but also inhibits sorbent sintering. As a result, excellent activity and stability were observed with up to 91% CH_4 conversion, >72% CO_2 capture efficiency and ~100% residue O_2 capture efficiency from flue gas by utilizing the $CeO_2 \leftrightarrow Ce_2O_3$ redox transitions, rendering an intensified process with zero coke deposition. Moreover, the SLDRM with $SrCe_{0.5}Ni_{0.5}$ has the flexibility to produce concentrated CO via CO_2-splitting while co-producing a syngas with tunable H_2/CO ratios.

1. Introduction

The increase in atmospheric CO_2 level is triggering adverse effect on climate, environment and ecosystem [1]. Although anthropogenic CO_2 emissions can be primarily ascribed to the utilization of fossil fuels, they are expected to remain as important energy sources within the foreseeable future [2]. Hence, CO_2 capture and utilization is of significant importance in the coming decades. International Energy Agency considers carbon capture and storage (CCS) as one of the key strategies to mitigate CO_2 emission in the short to intermediate term since it is applicable to large CO_2 sources like power plant, cement plant, etc. To date, extensive efforts have been committed to developing high performance sorbents for CO_2 removal, including grafted amine on porous materials [3-5], alkaline earth metal oxides [6-9], alkali metal-based salts [10-12], etc. However, the commercial application of CCS still faces challenges such as high capital cost, substantial energy penalty, and unreliable CO_2 storage technology.

An alternative strategy to CO_2 storage is to utilize the captured CO_2 to produce value-added chemicals or fuels. To convert CO_2, significant energy input and/or high temperature are required to activate the C=O bond. As a result, the energy efficiency for CO_2 utilization is limited [13-16]. Introducing a reducing agent such as methane can help to activate and rearrange the chemical bonds into target products. One such example is catalytic dry reforming of methane (DRM), which uses CH_4 to convert CO_2 into syngas, a mixture of H_2 and CO applicable for the synthesis of chemicals and fuels. Previous research has focused on the development of effective, coke-resistant DRM catalysts [17-22]. It is noted that DRM produces syngas with H_2/CO = 1/1, which still needs to be conditioned before further utilization in methanol or Fischer-Tropsch synthesis. In comparison, hybrid redox process, also known as chemical looping dry reforming of methane (CLDRM), produces syngas of H_2/CO = 2/1 and pure CO streams separately [23-25]. CLDRM uses oxygen carrier to divide DRM into two reaction steps, i.e., CH_4 partial oxidation to form CO and H_2 (MeO reduced to Me) and CO_2 splitting to form CO (Me oxidation to MeO). In CLDRM, the oxygen partial pressure (P_{O2}) of the oxygen carrier plays an important role towards the syngas selectivity [25]. In this aspect, CeO_2, a non-stoichiometric oxide [26, 27], exhibits desirable thermodynamic and kinetic properties for methane partial oxidation under a chemical looping scheme [28-30]. Overall, the key lies in the design of bifunctional materials for lattice oxygen storage/release and

[a] *Department of Chemical and Biomolecular Engineering, North Carolina State University, Raleigh, NC 27695-7905, United States.*
[b] *School of Energy and Power Engineering, Nanjing Institute of Technology, Nanjing 211167, China.*
[c] *Key Laboratory of Coal Gasification and Energy Chemical Engineering of Ministry of Education, Shanghai Engineering Research Center of Coal Gasification, East China University of Science and Technology, Shanghai 200237, China.*
**CO-corresponding authors.*
E-mail address: ygao9@ncsu.edu(Y. Gao), fli5@ncsu.edu (F. Li).
Electronic Supplementary Information (ESI) available: [details of any supplementary information available should be included here]. See DOI: 10.1039/x0xx00000x

catalysis that should have a good reaction affinity with both CO_2 and CH_4 [30-35].

Both DRM and CLDRM processes require a pure CO_2 feed, which is obtained from an energy intensive CO_2 capture step. Integrated sorbent looping and dry reforming of methane (SLDRM) has the potential to couple CO_2 capture and conversion steps, rendering an intensified process [36, 37]. Unlike DRM and CLDRM, SLDRM utilizes a sorbent to absorb CO_2 from flue gas. As is shown in Figure 1, the SLDRM process is implemented by cyclic carbonation and carbonate-CH_4 reforming in two separated, interconnected reactors. The sorbent is first carbonated to capture CO_2 from flue gas in the carbonation reactor and then, the CO_2-absorbed sorbent reforms CH_4 to produce syngas in the reforming reactor.

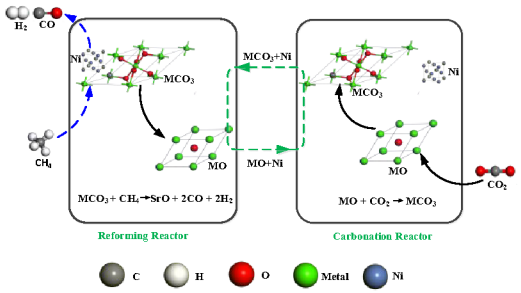

Figure 1. Schematic diagram of the integrated sorbent looping and dry reforming of methane (SLDRM).

Sorbent performance is the key factor that influences the efficiency of SLDRM. Extensive researches have been conducted to develop and optimize solid sorbent materials in the context of SLDRM, as are summarized in Table 1 [36-40]. Sung et al. [36] successfully demonstrated the process feasibility using lime sorbent particles at 720 °C, and the addition of Ni efficiently enhanced the CH_4 conversion. Tian et al. [37] also reported the combined process with a combined material of Ni-CaO, obtaining a similar catalytic effect of Ni. Unfortunately, performance deterioration was observed within 10 cycles for both sorbents. This was mainly ascribed to the low sintering resistance of CaO, which is a common problem facing the alkali-earth oxide sorbents [6, 7]. Hu et al. [38] used ZrO coating to stabilize CaO in the SLDRM process at 720 °C. However, CO_2 capacity and CH_4 conversion efficiency still decreased by 25% and 45% respectively within 10 cycles. Mendoza-Nieto et al. [39, 40] also investigated the SLDRM using Li_2ZrO_3 and Na_2ZrO_3, and stable H_2 production was obtained but with a low CH_4 conversion efficiency (15-20%). The results indicate that the mainstream SLDRM sorbents still face the problems of poor reactivity stability or lower CH_4 conversion. Additionally, no investigation involved O_2 containing flue gas (consistent with real flue gas). Overall, developing efficient absorbent is still the key task for the SLDRM process

Different from CaO which has desirable thermodynamic properties for CO_2 capture, SrO as a sorbent is generally considered infeasible due to the high stability of $SrCO_3$, which would require very high operating temperatures and/or limited CH_4 conversion in SLDRM. In this study, we propose to solve this issue by introducing a complex carbonation/decarbonation phase-transition using Ce-Sr interaction, i.e. $2SrCO_3 + CeO_2 \leftrightarrow Sr_2CeO_4 + 2CO_2$ as opposed to the conventional, simple carbonation/decarbonation cycles (e.g. $SrCO_3 \leftrightarrow SrO + CO_2$). This double replacement crystalline phase transition mechanism not only adjusts the carbonation/calcination thermodynamics to facilitate $SrCO_3$ decomposition at a relatively low temperature but also inhibits sorbent sintering. Another limitation of SLDRM is that it is a highly endothermic process, with the overall reaction ($CH_4 + CO_2 = 2CO + 2H_2$) has a heat of reaction of 259.12 kJ/mol at 850 °C. This can be mitigated by utilizing the residue O_2 from flue gas with the $CeO_2 \leftrightarrow Ce_2O_3$ redox transition, rendering an intensified process with zero coke deposition and decreased energy requirement. Moreover, the SLDRM with $SrCe_{0.5}Ni_{0.5}$ has the flexibility to produce concentrated CO via CO_2-splitting while co-producing a syngas stream with tunable H_2: CO ratios.

2. Experimental section

2.1. Materials Preparation

The $SrCe_{1-x}Ni_x$ sorbent catalysts were prepared using a modified Pechini method [41, 42]. All the chemical reagents were from Sigma-Aldrich, and a representative preparation process is described below. Initially, stoichiometric amount of $Sr(NO_3)_2$ (99.0%,), $Ce(NO_3)_3{\cdot}6H_2O$ (99%) and $Ni(NO_3)_2{\cdot}6H_2O$ (99.9%) were dissolved in deionized water at 80 °C. Citric acid (99.5%) and ethylene

Table 1. Summary of recent results on SLDRM.

Sorbent composition	Carbonation/DRM temperature	Cycle stability	Methane conversion*	H_2/CO	O_2-containing flue gas	Ref.
Ce/Ni-SrO	875/875 °C	Methane conversion, syngas selectivity and CO_2 update stabilized within 30 cycles	~100%	0.6-2, tunable	Yes	This study
Ni/MgO-Al_2O_3 + $CaCO_3$ composite	720/720 °C	CO_2 uptake decreased by 38% within 10 cycles	~100%	~1.1	No	31
Ni/CaO	600/800 °C	Both CH_4 and CO_2 conversion decreased by ~20% within 10 cycles	~100% in cycle 1	~1	No	32
NiCe/$CaCO_3$@ZrO_2	720/720 °C	CO_2 uptake decreased by ~30% within 10 cycles	90%-40%	~0.8	No	33
Li_2ZrO_3 and Na_2ZrO_3	400-600/900 °C	H_2 production rate stabilized within 6 cycles.	~15%	>>1	No	34
NiO(x)-Na_2ZrO_3	400-600/800-900 °C	H_2 production rate stabilized within 6 cycles.	~20%	1.1-2	No	35

* Given the differences in temperature, space velocity, and equilibrium constraints, methane conversion does not directly correspond to sorbent/catalyst activity.

ARTICLE

glycol (99.8%) were successively introduced at the molar ration of citric acid: ethylene glycol: cations (Sr^{2+}, Ce^{3+} and Ni^{2+}) = 3.75 : 2.5 : 1. The solution was kept stirring at 80 °C to form viscous gel, which was then dried at 180 °C to form a precursor. Finally, the precursor was calcined in a muffle furnace at 900 °C for 3 h. The calcined materials were crushed and double sieved to the size range of 0.1 - 0.3 mm. To be specific, the materials were named as $SrCe_{1-x}Ni_x$.

2.2. Sample Characterization

The chemical components of carbonated and reduced samples were determined by using a Rigaku SmartLab X-ray diffractometer (XRD) with Cu Ka (k = 0.15418 nm) radiation at 40 kV and 44 mA at room temperature. The XRD patterns were collected in the 2θ range of 10 - 90 ° with a step of 0.02 ° for 0.3 s. In-situ XRD analysis was also conducted to identify the phase transition of material during redox reactions. It was conducted in a Panalytical Empyrean X-ray diffractometer with a XRK900 (Anton Paar) reactor chamber, and phase patterns were collected in the 2θ range of 15-55 °. The sample was first heated from room temperature to 850 °C at a heating rate of 10 °C /min in N_2 atmosphere and then, isothermal redox reactions were carried out at 850 °C. Since coke deposition during CH_4 reforming may damage the instrument and therefore, the redox was carried out alternately using CO_2/N_2 and H_2/N_2 instead.

Surface morphology characterization of fresh samples (initially underwent H_2-reuduction and CO_2 carbonation) was conducted using scanning transmission electron microscope (TEM, FEI Talos F200, 300 kV). TEM was also used visualize the deposited carbon. The elemental distributions were simultaneously determined using energy dispersive spectrometry (EDS).

Raman spectra was determined using XploRA Plus Spectrometer with 532 nm wavelength. Each sample was scanned between 500 and 3500 cm^{-1} for 10 s to identify the type of deposited carbon on the sample.

2.3 Reactivity and Stability

H_2-TPR was carried out in a SDT 650 thermogravimetric analyzer (TGA) to evaluate the effect of Ce on $SrCO_3$ decarbonation process. To maintain the catalyst as metallic Ni, the sample initially successively underwent H_2 reduction and CO_2 carbonation. In each test, 20 mg of powder sample was loaded in an alumina crucible and exposed to 10% H_2 in Ar (200 mL/min). The temperature was increased to 950 °C at a heating rate of 10 °C/min.

Isothermal cycle carbonation/decarbonation at 875 °C was also conducted in the TGA to evaluate the reactivity stability of sorbent. 20% CO_2 in Ar (200 mL/min) and 20% H_2 in Ar (200 mL/min) were used in carbonation and decarbonation process, respectively.

CH_4-TPR was conducted in a U-tube reactor with 100 mg of carbonated sample in each test. The sample was exposed to 2.67% CH_4 in Ar (30 ml/min) and heated to 1000 °C at a rate of 10 °C /min. The outlet gas composition was online analyzed with a mass spectrum cirrus 2.

2.4. Integrated CO_2 Capture and CH_4 Reforming

Integrated CO_2 capture and CH_4 reforming was conducted with both residue O_2-containing flue gas and O_2-free CO_2 gas. The experiments were conducted in a U-tube with 0.5 g material in each test. In conducting the SLDRM with residue O_2-contained flue gas, the sample periodically exposed to 25 Vol. % flue gas (3 Vol.% O_2, 15 Vol. % CO_2 and 82 Vol. % Ar) in Ar during carbonation stage and 10 Vol. % CH_4 in Ar during reforming stage. The flow rate in the carbonation stage is flue gas/Ar = 10/30 sccm. And the flow rate in the reforming stage is CH_4/Ar = 3.3/30 sccm. A 2 min Ar of 30 sccm was used for purging between each stage. In conducting SLDRM with O_2-free CO_2 gas, the sample was first reduced by 25% H_2 in Ar at 850 °C for 2 h before the experiment. The sample was periodically exposed to 25 Vol. % CO_2 in Ar (10 sccm CO_2 and 30 sccm Ar) during carbonation stage and 10 Vol. % CH_4 in Ar (3.33 sccm CH_4 and 30 sccm Ar) during reforming stage. A 2 min Ar of 30 sccm was used for purging between each stage. The composition of product gas was online analyzed with Cirrus 2 mass spectrometer. The used materials at different reaction stages were also sampled for characterization. Some indexes are defined to evaluate the SLDRM process, including CH_4 conversion efficiency X_{CH_4}, overall H_2 yield Y_{H_2} and overall CO yield Y_{CO}, CO ratio in the reforming step S_{CO} and sorbent capacity C_{Sr}.

$$X_{CH_4} = 1 - \frac{F_{CH_4,out}}{F_{CH_4,in}} \quad \text{(E1)}$$

$$Y_{H_2} = 1 - \frac{F_{H_2}}{2(F_{CH_4,in} - F_{CH_4,out})} \quad \text{(E2)}$$

$$Y_{CO} = 1 - \frac{F_{CO}}{2(F_{CH_4,in} - F_{CH_4,out})} \quad \text{(E3)}$$

$$S_{CO} = \frac{F_{CO,reform}}{F_{CO,reform} + F_{CO2,reform}} \quad \text{(E4)}$$

$$C_{Sr} = 1 - \frac{F_{CO_2,actual}}{F_{CO_2,thoery}} \quad \text{(E5)}$$

Where $F_{CH_4,out}$ and $F_{CH_4,in}$ are flow rate of outlet CH_4 and input CH_4, respectively. F_{H_2} and F_{CO} are flow rate of H_2 and CO formation during the cycle, respectively. $F_{CO,reform}$ and $F_{CO2,reform}$ are the flow of CO and CO_2 during the reforming step. $F_{CO_2,cap}$ and $F_{CO_2,thoery}$ are the amount of CO_2 actually captured and CO_2 that sorbent could captured.

3. Results and Discussion

3.1. Stability of the Ce Incorporated Sorbent

Sorbent stability is arguably the most important property for sorbent design. Figure 2 shows the cyclic carbonation/decarbonation process using the sorbents with and without CeO_2 incorporation. Similar to other alkali earth based sorbents, significant activity

deterioration occurred to SrNi, and the sorbent capacity decreased from 100% to about 20% after 35 cycles. This indicates that Ni addition, while effective to enhance methane activation, cannot prevent sintering caused by direct phase transition of SrO/$SrCO_3$. This reactivity deterioration trend due to direct oxide/carbonate transition are similar to various CaO based sorbents [6-9]. In contrast, CeO_2 incorporation and interaction between CeO_2 and SrO substantially improved the sorbent stability. The sorbent capacity of $SrCe_{0.5}Ni_{0.5}$ maintained almost unchanged during the entire 35 cycles, and a near 100% capacity was obtained. This is highly encouraging because the incorporation of CeO_2 provides a potential solution to sorbent stability challenges.

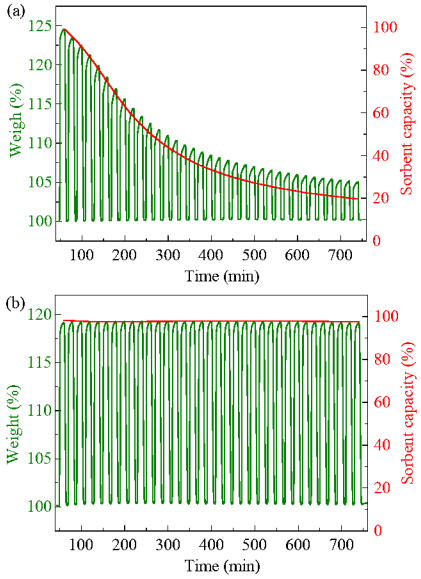

Figure 2. TGA profiles of 35 carbonation/decarbonation cycles at 875 °C with 20%CO_2 and 20%H_2 using (a) SrNi and (b) $SrCe_{0.5}Ni_{0.5}$.

3.2. Phase Transition and Surface Morphology

Ex-situ XRD patterns were collected from the pre-reduced and pre-carbonated sorbents to identify the crystal phases of the sorbents at these two specific states (Figure 3). The diffraction peaks of metallic Ni was observed in both samples, indicating that a fraction of the Ni can dissociate from the mixed oxide/carbonate sorbent as the active sites for CH_4 conversion. $SrCO_3$ in the sorbent would cover NiO and lead to incomplete reduction of NiO during the pretreatment process. Therefore, weak diffraction peaks of NiO were also observed (Figure 2b). Although the sorbents have varying Ce content, the main components in these carbonated samples were $SrCO_3$ and CeO_2 in all cases. Sr_2CeO_3 was formed during the decarbonation process, and Ce-lean samples would trigger the formation of SrO whereas Ce-rich samples have $SrCeO_3$ and CeO_2 phases present. The diffraction peaks of $Sr(OH)_2$ instead of SrO in the sample was resulted from exposure to the moisture in ambient air. As a comparison, Figure 3c shows the *in-situ* XRD analysis of $SrCe_{0.5}Ni_{0.5}$ during reduction (5%H_2/N_2) and carbonation (20% CO_2/N_2) at 850 °C. $SrCO_3$ and CeO_2 were observed in the carbonation process, and $SrCeO_3$ and Sr_2CeO_4 were formed in the decarbonation process. Hence, the reversible interaction between CeO_2 and $SrCO_3$ during carbonation/decarbonation cycle can be described by (R1) and (R2). The elevated temperature and the lower CO_2 pressure favor the formations of $SrCeO_3$ and Sr_2CeO_4 [43, 44], both of which also depend on the Sr:Ce ratio. The minority phases, i.e., CeO_2, SrO, can be avoided by maintaining an Sr:Ce ratio near 2:1. The Overall, the direct phase change between $SrCO_3$ and SrO can be completely avoided by introducing the intermediate $SrCeO_3$/Sr_2CeO_4 phases, which inhibits sorbent sintering via cation migrations that are required for intermediate phase formation.

Carbonation: $SrCeO_3/Sr_2CeO_4+CO_2 \rightarrow SrCO_3+CeO_2$ (R1)

Decarbonation: $SrCO_3+CeO_2 \rightarrow SrCeO_3/Sr_2CeO_4+CO_2$ (R2)

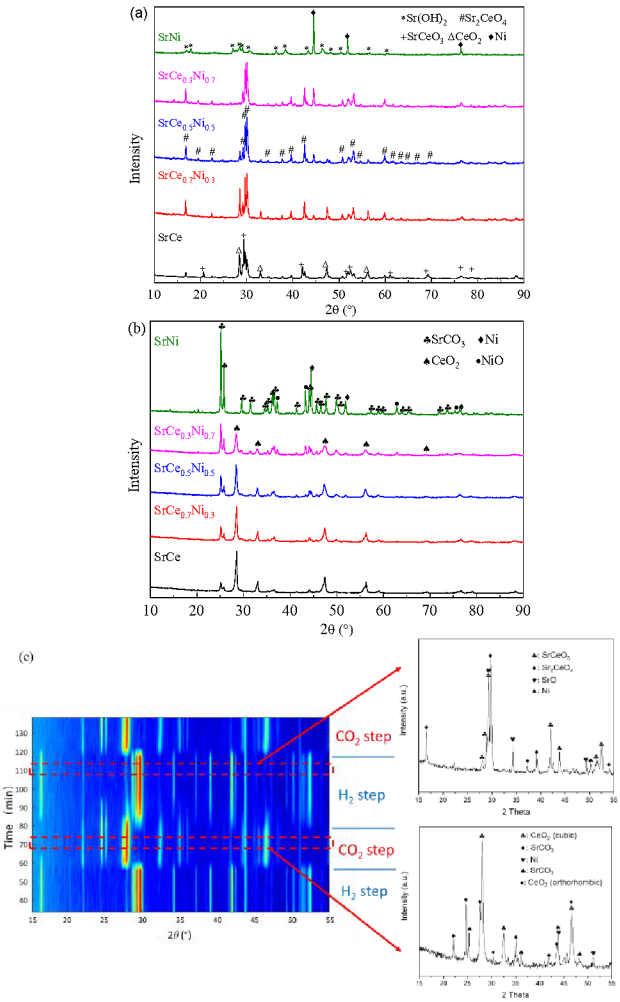

Figure 3. XRD patterns of sorbent at different state: (a) decarbonated $SrCe_{1-x}Ni_x$, (b) carbonated $SrCe_{1-x}Ni_x$ and (c) *in-situ* XRD of $SrCe_{0.5}Ni_{0.5}$.

H_2-TPR was conducted with the pre-carbonated sorbents to evaluate the effect of CeO_2 incorporation on the decarbonation reactivity. Figure 4 shows the reaction profiles of pre-carbonated $SrCe_{1-x}Ni_x$. The reaction rate gradually increased after 700 °C, and then decreased after about 890 °C depending on the Ce content. Higher Ce loading caused the reaction peak shift to lower temperatures. The reaction peak shifted from about 910 °C for SrNi to about 850 °C for SrCe, along with increase in the peak sizes. This

indicates that the solid states interaction between CeO_2 and $SrCO_3$ (R2) facilitated the decarbonation process at a lower temperature rather than at an extremely high temperature for traditional thermal decomposition of $SrCO_3$. This is understandable since the formation of mixed Sr/Ce oxide, which is more thermodynamically stable in the sorbent, would enhance the decarbonation reaction from a thermodynamic standpoint in additional to its ability to inhibit sintering. This also indicates that the integrated decarbonation and CH_4 reforming can be potentially operated at a lower temperature with the Ce-supported Sr-based sorbent.

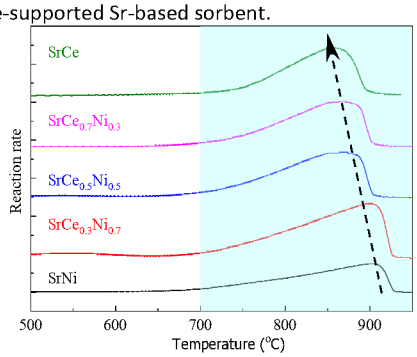

Figure 4. H_2-TPR profile of the pre-carbonated $SrCe_{1-x}Ni_x$ under 10%H_2 at a heating rate of 10 °C/min. In prior to H_2-TPR, the sample underwent reduction (25% H_2 for 4 h) to obtain metallic Ni and carbonation (25% CO_2 for 2 h) at 800 °C.

The XRD and H_2-TPR characterizations indicate that $SrCe_{0.5}Ni_{0.5}$ is likely to be a promising sorbent material. Therefore, carbonated SrNi and $SrCe_{0.5}Ni_{0.5}$ were selected to investigate the effect of Ce on the surface morphology, with Figure 5 showing the TEM-EDX analysis results. The lattice morphology images (Figure 5b and 5e) clearly show that the carbonated SrNi sorbent contained $SrCO_3$ and Ni, while the carbonated $SrCe_{0.5}Ni_{0.5}$ contains $SrCO_3$, Ni and CeO_2. It indicates that Sr-based sorbent could be well converted to $SrCO_3$ during the carbonation process. However, EDX mapping of main elements in Figures 5c and 5f exhibits two typical surface morphology features for SrNi and $SrCe_{0.5}Ni_{0.5}$. Clusters of Ni can be observed on SrNi particles surface, which indicates Ni aggregation. In comparison, the addition of CeO_2 promoted more uniform distribution of Ni as evidenced by the absence of clustering on the surface of $SrCe_{0.5}Ni_{0.5}$. It is proposed that the interactions among CeO_2, SrO, and Ni are beneficial for Ni dispersion.

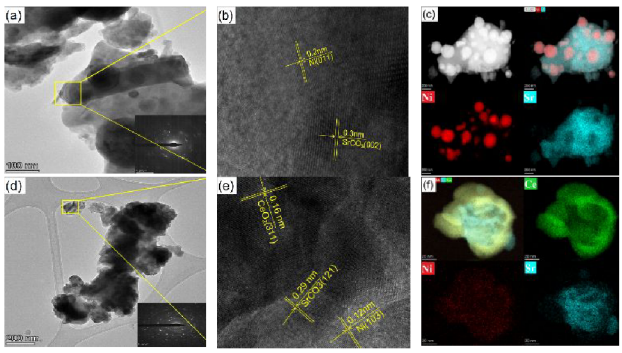

Figure 5. TEM-EDX analysis of SrNi: (a) TEM image, (b) HRTEM image of yellow rectangle in Figure a, (c) element distribution according to EDX mapping; and $SrCe_{0.5}Ni_{0.5}$: (d) TEM image, (e) HRTEM image of yellow rectangle in Figure d, (f) element distribution according to EDX mapping.

3.3. Synergy of Ce and Ni for Sorbent-CH_4 Reactions

CH_4-TPR was conducted using carbonated sorbents and the gaseous products are shown in Figure 6. The CH_4 conversion is highly dependent on the bed materials. In the case of SrCe in figure 6a, CO_2 appeared above 800 °C, peaking at about 920 °C and most CH_4 was not converted. This means that CO_2 released from $SrCO_3$ can barely participate in CH_4 reforming below 1,000 °C without Ni. In contrast, CH_4 reforming occurred on SrNi sorbent during 850-950 °C in Figure 6b. H_2/CO=~1 was obtained during the early stage of the reaction. Slight CH_4 cracking also occurred on the CO_2-exhausted sorbent, generating more H_2 than CO. To be noted, a comparable CO_2 concentration also appeared in this stage, indicating incomplete CO_2 conversion during the DRM process, which strongly depends on the catalyst activity. The utilization of $SrCe_{0.3}Ni_{0.7}$, $SrCe_{0.5}Ni_{0.5}$ and $SrCe_{0.7}Ni_{0.3}$ significantly changed the CH_4 conversion performance, as are shown in Figures 6c - 6e. Due to methane cracking, notable H_2 formation was observed at low temperatures (380-680 °C) with little CO formation. This could be attributed to: (1) the presence of Ni/CeO_x interface was shown to be highly effective for methane activation at lower temperatures [45-49]. (2) The oxygen vacancies and high mobility of lattice oxygen associated with ceria are conducive to CH_4 activation [50-53]. With temperature increasing to ~800 °C, the modified water-gas shift reaction, i.e. $H_2 + SrCO_3 = SrO + H_2O + CO$, becomes more favourable thermodynamically, leading to H_2/CO <1. Further increase in temperature caused more severe methane cracking reaction with H_2/CO >1. Up to ~100% CH_4 conversion was obtained and the peaks of H_2 and CO appeared at lower temperatures (800-900 °C) when compared to SrNi. Simultaneously, CO_2 maintained at a negligible level during the whole stage, indicating that the released CO_2 can fully participate in CH_4 reforming when using the both Ce and Ni tuned sorbent. Overall, the Ni-Ce interaction facilitated sorbent and CH_4 conversion.

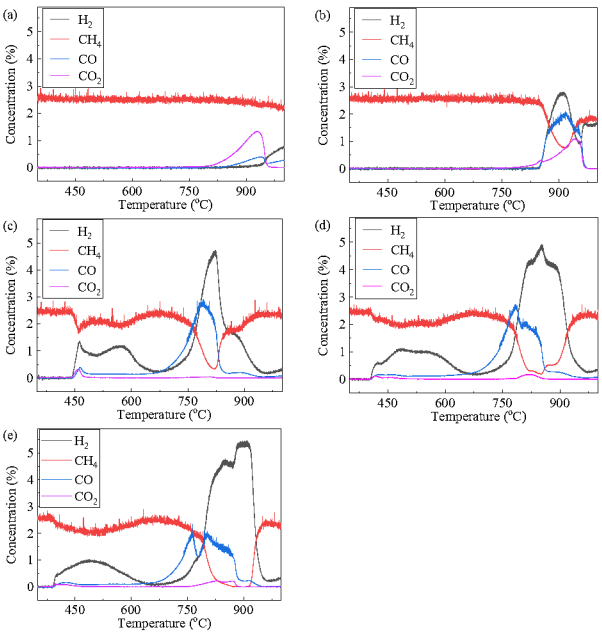

Figure 6. Gas product evolution during CH_4-TPR profile with carbonated sorbent: (a) SrCe, (b) SrNi, (c) $SrCe_{0.7}Ni_{0.3}$ (d) $SrCe_{0.5}Ni_{0.5}$ (e) $SrCe_{0.3}Ni_{0.7}$. These materials all underwent reduction (25% H_2 for 2 h) and carbonation (25% CO_2 for 2 h) at 800 °C prior to CH_4-TPR.

Figure 7 compares the decarbonation rate of SrCe and $SrCe_{0.5}Ni_{0.5}$ at 875 °C with and without CH_4. Although the CeO_2 addition enhanced CO_2 release, decarbonation rate of both materials in Ar atmosphere was still very low at 875 °C. It means that a higher temperature is necessary for thermal decomposition of $SrCO_3$. Furthermore, the decarbonation rate of SrCe in CH_4 atmosphere was also very low, and it indicates that SrCe was inactive for CH_4 reforming without Ni catalyst. As anticipated, a significant increase in decarbonation rate was observed for $SrCe_{0.5}Ni_{0.5}$ in CH_4 as compared to that in N_2. Overall, the $SrCe_{0.5}Ni_{0.5}$ exhibited a superior decarbonation rate during the SLDRM. Hence, it provides an opportunity for $SrCO_3$ decarbonation at a lower temperature.

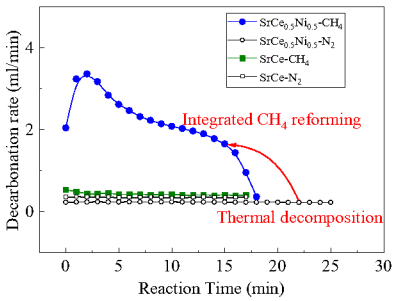

Figure 7. Decarbonation rate of SrCe and $SrCe_{0.5}Ni_{0.5}$ at 875 °C with and without CH_4.

3.4. Isothermal SLDRM with O_2-containing Flue Gas

As discussed above, SLDRM is a highly endothermic process, with a reaction heat of 259.12 kJ/mol at 850 °C. With CaO-based absorbent, SLDRM also requires temperature swing for CO_2 capture and reforming, leading to additional energy input. The proposed $SrCe_{1-x}Ni_x$ oxide can eliminate the need for temperature swing, and mitigate the issue for endothermicity by utilizing the residue O_2 in flue gas with the $CeO_2 \leftrightarrow Ce_2O_3$ redox pair. As discussed above, both decarbonation and methane reforming steps with $SrCe_{1-x}Ni_x$ happened at above 800 °C, making it feasible for an isothermal cyclic process. Here, we chose 875 °C as the optimal temperature for SLDRM. Figure 8(a) shows the gas evolution during a typical CH_4-flue gas cycle using $SrCe_{0.5}Ni_{0.5}$. The overall methane conversion in the reforming step was 90.7%, indicating that the oxygen in the flue gas did not cause observable negative influence on the activity of Ni. At the initial stage of the reforming step, the instantaneous H_2/CO ratio was close to 1.5, indicating that the methane partial oxidation reaction was dominant. Then, CO flow rate increased and the instantaneous H_2/CO ratio decreased to about 1, indicating that methane carbonate dry reforming began to take place. The overall H_2/CO ratio in the reforming step is 1.21. It is noted that although Ni is still present, the participation of CeO_2 in methane reforming provides active oxygen species, which can inhibit coke formation [53]. The lack of coke deposition was also exhibited via flue generation in the carbonation-oxidation step. As can be seen, no CO was formed during the carbonation step and the CO_2 capture efficiency from flue gas was 72.4%. Moreover, all residue O_2 in the flue gas has been utilized and the participation of O_2 can improve the heat management of the highly endothermic SLDRM process, as methane partial oxidation was an exothermic reaction. The stability of the isothermal SLDRM with O_2-containing flue gas was confirmed by running 20 CH_4-flue gas cycles on $SrCe_{0.5}Ni_{0.5}$. As can be seen in Figure 8b, the performance was highly stable over the 20 cycles for integrated CO_2 capture and conversion.

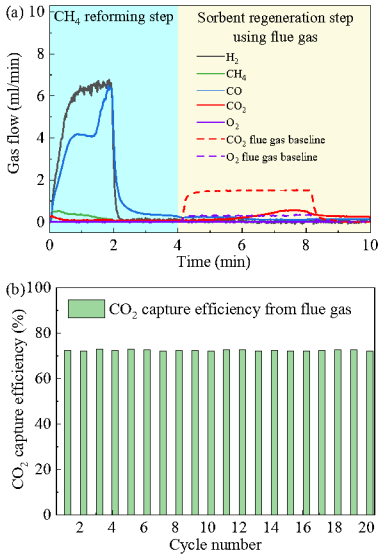

Figure 8. (a) A typical gas product distribution of SLDRM with $SrCe_{0.5}Ni_{0.5}$ under CH_4-flue gas cycles at 875 °C, dashed lines stand for blank gas flow at room temperature with no sorbents in reactor; (b) CO_2 capture efficiency from flue gas of $SrCe_{0.5}Ni_{0.5}$ under 20 CH_4-flue gas cycles at 875 °C.

3.5. Isothermal SLDRM with O_2-free CO_2

Besides isothermal SLDRM with O_2-containing flue gas, isothermal SLDRM was also explored using O_2-free CO_2. Figure 9a compares the effect of sorbent on CH_4 conversion at typical temperatures (800-900 °C). Higher temperature leads to higher CH_4 conversion for all these samples. Standalone SrCe was nearly inactive for CH_4 activation at all temperatures, i.e., with CH_4 conversion less than 2%. SrNi was more active than SrCe yet the CH_4 conversion was still below 90%. In comparison, $SrCe_{1-x}Ni_x$ exhibited a synergistic effect in promoting CH_4 conversion and near 100% conversion was obtained above 875 °C for $SrCe_{0.5}Ni_{0.5}$ and $SrCe_{0.3}Ni_{0.7}$. This again confirms the synergy between Ce and Ni for CH_4 conversion. One of the best-performing samples, $SrCe_{0.5}Ni_{0.5}$, was selected for cyclic stability test, as demonstrated by Figures 9b-9d. Figure 9b showed gas evolution during one typical cycle of SLDRM at 875 °C. The outlet CH_4 flow maintained at a negligible value, and nearly 100% conversion was obtained during the reforming process. At the beginning of the reforming step, the instantaneous flow rate of H_2 and CO were almost equivalent, indicating that methane-carbonate dry reforming was the dominate reaction. After 2 mins, the CO flow rate decreased while H_2 flow rate remained almost the same and the instantaneous H_2/CO ratio gradually increased to almost 2. This indicated that both coke deposition and carbonate dry reforming

occurred at the later stage of the reforming step. The formation of deposited carbon was further confirmed with TEM and Raman, showing mainly graphitic carbon formations on top of Ni-containing sorbents (Figures S1 and S2). Despite of the relative stability of the graphitic carbon, the coke was completely removed during the subsequent carbonation process. The facile coke removal was likely to be due to the catalytic effect of Ni-Ce [54]. A large CO peak was obtained during the initial carbonation stage from 12 min to 14 min. Simultaneously, CO_2 absorption process occurred from 12 min to 16 min. As a result, CO_2 was barely observed during this stage. The sorbent exhibited an excellent cyclic performance at 875 °C within 30 cycles, as shown in Figure 9c and Figure 9d. The sorbent capacity C_{sr} and CH_4 conversion maintained above 63% and above 98%, respectively. The overall yield of H_2 and CO was ~89% and 111% during the 30 cycles. The difference between them and the CO yield exceeded 100% can be ascribed to the reverse water gas shift reaction. The overall syngas yield (H_2+CO) maintained at about 100%. The microstructure and phase integrity after 30 cycles were examined with SEM and XRD, showing good stability of the sorbent (Figures S3 and S4). Moreover, the H_2/CO ratio could be tuned by changing the methane injection time during the reforming step. As can be seen in Figure 8e, the H_2/CO ratio monotonously decreased from 1.91 to 0.63 with methane duration decreased from 10 to 0.5 min. The ratio of H_2/CO <1 could be ascribed to the reverse water gas shift reaction. To produce a pure CO stream in the CO_2 utilization/carbonation step, the carbonation step time was adjusted. Figure 9f shows the gas evolution during typical SLDRM process with 20 mins reforming step and 6.66 mins carbonation step. It was observed that an almost 100% pure CO stream was obtained at the CO_2 utilization/carbonation step. This allows effective CO_2 utilization with tunable H_2/CO ratio and a separate highly pure CO stream during the SLDRM without further syngas conditioning units. Overall, the $SrCe_{0.5}Ni_{0.5}$ presents excellent flexibility in SLDRM with tunable H_2/CO ratios. O_2-intensified SLDRM using residue O_2 from flue gas was also feasible, as elaborated in Section 3.4. It is interesting to note that the presence of residue O_2 in fossil fuel combustion flue gas inhibited coke formation on the catalytic sorbent whereas the same sorbent acts as a dual function carbon/oxygen carrier in absence of the residue O_2. This unique property, which can be attributed to the size and oxidation state of the surface Ni sites under the different oxidizing environments, offers excellent potential for a wide range of application scenarios.

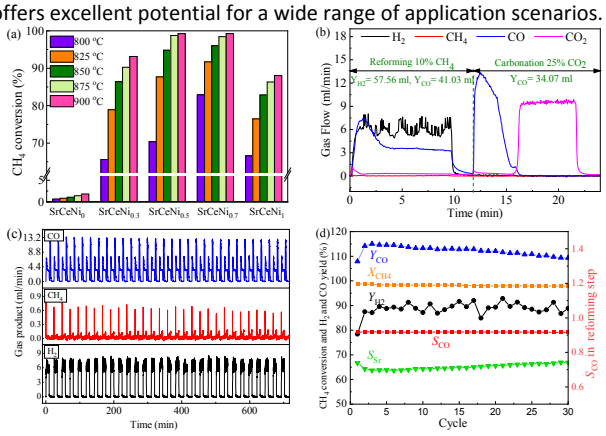

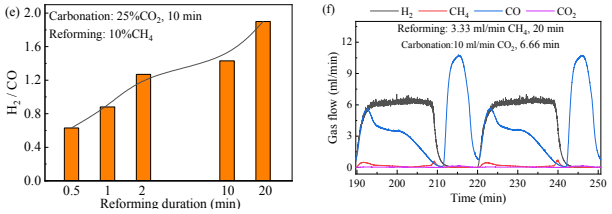

Figure 9. Isothermal SLDRM performance using $SrCe_{1-x}Ni_x$: (a) effect of sorbent on CH_4 conversion at typical temperature, and cycle performance of $SrCe_{0.5}Ni_{0.5}$ at 875 °C of (b) gas evolution in a typical cycle, (c) overall view of gas products in 30 cycles, (d) main indexes in the reforming step during 30 SLDRM cycles, (e)effect of methane duration on H_2/CO ratio, (f) gas evolution during SLDRM cycle with almost 100% CO formation during the carbonation step and (g) A schematic drawing showing the versatility of SLDRM using $SrCe_{1-x}Ni_x$.

Conclusions

To summarize, catalytic phase transition sorbents composed of Ni promoted and Ce stabilized SrO was synthesized and characterized for SLDRM. The addition of CeO_2 functioned as a dispersant, rendering an even distribution of Ni catalyst in the material. Moreover, the Ce-Sr interaction promoted a complex carbonation/decarbonation phase-transition, i.e. $SrCO_3 + CeO_2 \leftrightarrow Sr_2CeO_4 + CO_2$ as opposed to the conventional, simple carbonation/decarbonation cycles (e.g. $SrCO_3 \leftrightarrow SrO + CO_2$). This double replacement crystallite phase transition mechanism not only adjusted the carbonation/calcination thermodynamics to facilitate $SrCO_3$ decomposition at relatively low temperatures but also inhibits sorbent sintering. As a result, excellent activity and stability were observed with up to 91% CH_4 conversion, >72% CO_2 capture efficiency and ~100% residue O_2 capture efficiency from flue gas by utilizing the $CeO_2 \leftrightarrow Ce_2O_3$ redox transitions, rendering an intensified process with zero coke deposition and improved endothermicity. Moreover, the $SrCe_{0.5}Ni_{0.5}$ catalytic sorbent can also convert an O_2-free CO_2 stream to CO and produce syngas with tunable H_2/CO ratio by adjusting the methane reforming step time. Overall, this study reports a new approach to design effective phase-transition materials for stable SLDRM with tunable product compositions. The utilization of redox pairs in the O_2-intensified SLDRM approach with real combustion flue gas also shed light on future opportunities for process intensification in the context of CO_2 capture and conversion.

Author Contributions

Haiming Gu: Investigation, Writing – original draft preparation. Yunfei Gao: Conceptualization, Writing – review & editing, Supervision. Sherafghan Iftikhar: Writing – review & editing. Fanxing Li: Conceptualization, Writing – review & editing, Supervision, Project administration, Funding acquisition.

Conflicts of interest

There are no conflicts to declare.

Acknowledgements

This work was supported by the US National Science Foundation (CBET-1923468), the US Department of Energy (EE0008809), and Kenan Institute of Engineering, Technology, and Science.

References

[1]https://climate.nasa.gov/vital-signs/carbon-dioxide/
[2] M. Marien, *World future rev*., 2012, **4(4)**, 90-95.
[3] S. B. Peh and D. Zhao, *Science*, 2020, **369(6502)**, 372-373.
[4] B. Ghalei, K. Sakurai, Y. Kinoshita, K. Wakimoto, A. Isfahani, Q. Song, K. Doitomi, S. Furukawa, H. Hirao, H. Kusuda, S. Kitagawa and E. Sivaniah, *Nature Energy*, 2017, **2(7)**, 17086.
[5] X. Si, C. Jiao, F. Li, J. Zhang, S. Wang, S. Liu, F. Xu and Z. Gabelica. *Energy Enviro*n. Sci., 2011, **4**, 4522-4527.
[6] D. P. Hanak, C. Biliyok and V. Manovic, *Energ. Environ. Sci.*, 2016, **9(3)**, 971-983.
[7] H. Sun, J. Wang, X. Liu, B. Shen, C. M. A. Parlett, G. O. Adwek, E. J. Anthony, P. T. Williams and C. Wu, J. Mater. Chem. A, 2019, **7(16)**, 9977-9987.
[8] A. Perejón, L. M. Romeo, Y. Lara, P. Lisbona, A. Martínez and J. M. Valverde, *Appl. Energ*., 2016, **162**, 787-807.
[9] Y. Hu, Y. Guo, J. Sun, H. Li and W. Liu, *J. Mater. Chem. A*, 2019, **7(35)**, 20103-20120.
[10] J. Ma, J. Zhong, X. Bao, X. Chen and C. Liang, *Chem. Eng. J.*, 2020, **404**, 126465.
[11]P. V. Subha, B. N. Nair, V. Vijayan, S. C.Ramakrishnan and H. Saraswathy, *J. Mater. Chem. A*, 2018, **6(17)**, 7913-7921.
[12] W. Ye, J. Lin, H. T. Madsen, E. G. Sogaard and B. Bruggen, *J. Membrane Sci.*, 2016, **498**, 75-85.
[13] C. Mesters, *Annu. Rev. Chem. Biomol. Eng*., 2016, **7(1)**, 223–238.
[14] S. C. Peter, *ACS Energy Lett.*, 2018, **3(7)**, 1557–1561.
[15] A. J. Carrillo, A. H. Bork, T. Moser, E. Sediva, Z. D. Hood and J. L. M.Rupp, *Adv. Energy Mater.*, 2019, **9(28)**, 1803886.
[16] I. Al-Shankiti, B. D. Ehrhart and A. W. Weimer, *Sol. Energy,* 2017, **156**, 21–29.
[17] Z. Bian and S. Kawi, *ChemCatChem*, 2018, **10**, 320-328.
[18] J. Zhang and F. Li, *Appl. Catal. B*, 2015, **176-177**,513-521.
[19] S.A. Theofanidis, V.V. Galvita, H. Poelman, N.V.R.A. Dharanipragada, A. Longo, M. Meledina, G. Van Tendeloo, C. Detavernier and G.B. Marin, *ACS Catal.*, 2018, **8**, 5983-5995.
[20] M. Akri, S. Zhao, X. Li, K. Zang, A.F. Lee, M.A. Isaacs, W. Xi, Y. Gangarajula, J. Luo, Y. Ren, Y.T. Cui, L. Li, Y. Su, X. Pan, W. Wen, Y. Pan, K. Wilson, L. Li, B. Qiao, H. Ishii, Y.F. Liao, A. Wang, X. Wang and T. Zhang, *Nat. Commun.*, 2019, **10(5181)**, 1-10.
[21] Z. Bian, I.Y. Suryawinata and S. Kawi, *Appl. Catal. B*, 2016, **195**, 1-8.
[22] N. A. K. Aramouni, J. G.Touma, B. A. Tarboush, J. Zeaiter and M. N.Ahmad, *Renew. Sust. Energ. Rev*., 2018, **82**, 2570-2585.
[23] S. Bhavsar, M. Najera and G. Veser, Chem. Eng. Technol., 2012, 35, 1281-1290.
[24] A. More, G. Veser and S. Bhavsar, *Energy Technol*., 2016, **4(10)**, 1147-1157.
[25]V. P. Haribal, F. He, A. Mishra and F. Li, *ChemSusChem*, 2017, **10(17)**, 3402-3408.
[26]B. Bulfin, A. J. Lowe, K. A. Keogh, B. E. Murphy, O. Lübben, & S. A. Krasnikov and I.V. Shvets, *J. Phys. Chem. C*, 2013, **117(46)**, 24129-24137.
[27] R. Schäppi, D. Rutz, F. Dähler, A. Muroyama, P. Haueter, J. Lilliestam, A. Patt, P. Furler and Aldo Steinfeld, *Nature*, 2021.
[28]L. Sun, K. Li, Y. Wei, X. Zhu and H. Wang, *Energ. Fuels*, 2014, **28(2)**, 754–760]
[29]Y. Zheng, K. Li, H. Wang, D. Tian, Y. Wang, X. Zhu, Y. Wei, M. Zheng and Y. Luo, *Appl. Catal. B*, 2017, **202**, 51-63.
[30] V. Haribal, X. Wang, R. Dudek, C. Paolus, B. Turk, R. Gupta and F. Li, *Adv. Energy Mater*., 2019, **1901963**, 1-10.
[31] J. Zhang, V. Haribal and F. Li, *Sci. Adv*., 2017, **3(8)**, e1701184.
[32] Q. Jiang, Y. Gao, V. Haribal, H. Qi, X. Liu, H. Hong, H. Jin and F. Li, *J. Mater. Chem. A*, 2020, **8**, 13173-13182.
[33] S. Iftikhar, Q. Jiang, Y. Gao, J. Liu, H. Gu, L. Neal and F. Li. *Energ. Fuel.,* 2021, **35(17)**, 13921–13929
[34]A. Lofberg, J. Guerrero-Caballero, T. Kane, A. Rubbens and L. Jalowiecki-Duhamel, *Appl. Catal. B*, 2017, **212**,159-174.
[35]M. Tang, K. Liu, D.M. Roddick and M. Fan, *J. Catal.,* 2018, **368,** 38-52.
[36] S. M. Kim, P. M. Abdala, M. Broda, D. Hosseini, C. Copéret and C. Müller, *ACS Catal*., 2018, **8(4),** 2815-2823.
[37] S. Tian, F. Yan, Z. Zhang and J. Jiang, *Sci. Adv*., 2019, **5(4)**, eaav5077.
[38] J. Hu, P. Hongmanorom, V. V. Galvita, Z. Li and S. Kawi, *Appl. Catal. B*, 2021, **284**, 119734.
[39] J. A. Mendoza-Nieto, Y. Duan and P. Heriberto, *Appl. Catal. B*, 2018, **238**, 576-585.
[40] J. A. Mendoza-Nieto, S. Tehuacanero-Cuapa, J. Arenas-Alatorre and H. Pfeiffer, *Appl. Catal. B*, 2018, **224**, 80-87.
[41] S. Chen, L. Zeng, H. Tian, X. Li and J. Gong, *ACS Catal*., 2017, **7**, 3548-3559.
[42] Y. Gao, L.M. Neal and F. Li, *ACS Catal*., 2016, **6 (11)**, 7293–7302.
[43] A. N. Shirsat, K.N.G. Kaimal, S. R. Bharadwaj and D. Das,J. *Solid State Chem*., 2004, **177(6),** 2007-2013.
[44] A. N. Shirsat, K.N.G. Kaimal, S. R. Bharadwaj and D. Das, *Thermochim. Acta*, 2006, **447(1)**, 101-105.
[45]Z. Liu, D.C. Grinter, P.G. Lustemberg, T.D. Nguyen-Phan, Y. Zhou, S. Luo, I. Waluyo, E.J. Crumlin, D.J. Stacchiola, J. Zhou, J. Carrasco, H.F. Busnengo, M. V. Ganduglia-Pirovano, S.D. Senanayake and J.A. Rodriguez, *Angew. Chem. Int. Ed. Engl*., 2016, **55**, 7455–7459.
[46] S. Das, J. Ashok, Z. Bian, N. Dewangan, M.H. Wai, Y. Du, A. Borgna, K. Hidajat and S. Kawi, *Appl. Catal. B*, 2018, **230**, 220–236.
[47] M. Li and A.C. van Veen, *Appl. Catal. B*, 2018, **237**, 641–648.
[48] S.P. Padi, L. Shelly, E.P. Komarala, D. Schweke, S. Hayun and B.A. Rosen, *Catal. Commun.,* 2020*,* **138 (105951)**, 1–5.
[49] Z. Liu, P. Lustemberg, RA Gutiérrez, J. J. Carey, R. M. Palomino, M. Vorokhta, D.C. Grinter, P.J. Ramírez, V. Matolín, M. Nolan, M Verónica,G. Pirovano, S. D,Senanayake and J.A. Rodriguez, *Angew. Chem. Int. Ed. Engl*., 2017, **56**, 13041-13046.
[50]F. Pan, X. Xiang, Z. Du, E. Sarnello, T. Li, Y. Li, *Appl. Catal. B*, 2020, **260**, 118189.
[51] T. Ye，W. Huang，L. Zeng, M. Li，J. Shi, *Appl. Catal. B*, 2017, **210,** 141-148.
[52] C. Okolie, Y. Lyu, L. Kovarik, E. Stavitski and C. Sievers, *ChemCatChem,* 2018, **10(12)**, 2700-2708.
[53]F. Pan, X. Xiang, W. Deng, H. Zhao, X. Feng, and Y. Li, *ChemCatChem*, 2018, **10(5)**, 940-945.
[54]B. Sellers-Antón, E. Bailon-Garcia, A. Cárdenas-Arenas, A. Davó-Quiñonero, D. Lozano-Castello, A. Bueno López, *Environ. Sci. Technol.*, 2020, **54(4)**, 2439-2447.

